Improved integro-modal approach with pressure distribution assessment and the use of overlapped cavities

E. Anyunzoghe[a], L. Cheng[b],*

[a]*Department of Mechanical Engineering, Laval University, Québec, Canada G1K 7P4*
[b]*Department of Mechanical Engineering, The Hong Kong Polytechnic University, Hong Kong*

Abstract

An integro-modal approach was previously developed in order to compute the normal modes of an acoustic enclosure of any shape. Though good approximation was achieved for estimating the natural frequencies, we show in this paper that improvement is still needed to ensure good pressure gradient continuity, which is crucial for the convergence of the numerical expression of the pressure distribution into the whole cavity. The technique of overlapped cavities is introduced in the general eigenvalue equations derived from the integro-modal theory. Numerical tests are performed to assess both the original and the modified approach, with special focus on the pressure approximation. The agreement between theoretical or other existing results and numerical solutions using the new approach is improved, in comparison to the results observed with the original approach. © 2002 Elsevier Science Ltd. All rights reserved.

1. Introduction

Most interior noise problems involve acoustic cavities of irregular shapes. The prediction of the modal characteristics of such enclosures is fundamental to a better understanding of the system behavior before any control action is taken. Apart from the classical boundary element method [1] and the finite element method [2], which are believed to be very general and versatile, others alternatives have also been proposed.

---

* Corresponding author. Tel.: +852-2766-6769; fax: +852-2365-4703.
E-mail address: mmlcheng@polyu.edu.hk (L. Cheng).

Relevant references on the related subjects may be found in Ref. [3]. More recent development has been reviewed by Levine in his recent paper [4]. Typical work includes the point-matching method [5], method using waveguide-type base functions [6,7] and the Integro-modal approach (IMA) [3]. The IMA was suggested to compute the acoustic modal properties of irregular cavities, where the separation of variable technique cannot be applied. The present paper presents a further assessment and improvement of the IMA.

Acousto-Elastic Method (AEM) [8] and Green Function Method (GFM) [9] inspired the Integro-modal approach. It consists in handling the irregular shaped enclosure as a multi-connected cavity system, with either regular or irregular sub-volumes. Minimal subdivision was striven. The modal characteristics of regular sub-cavities were obtained analytically, while irregular ones were treated using normal modes of their respective regular bounding cavities with rigid walls. In both cases, rigid-wall modes were used as base functions for a modal expansion of the sound field in the sub-cavity. The integral formulation ensured global continuity of the pressure between adjacent sub-cavities. The method then yielded a truncated eigenvalue system. Fewer sub-cavities were needed to obtain comparable results as other existing methods, in term of natural frequencies. The technique was used to compute the natural modes of a two-dimensional aircraft fuselage.

The previous work mainly focused on the prediction of natural frequencies. No study in terms of the corresponding modal pressures was performed. However, in many respects, modal pressure (or mode shape) is one of the most essential parameters to be known. First, the mode shape of acoustic cavities is usually used in vibro-acoustic analyses of vibrating structures coupled to an acoustic enclosure [10] In these cases, the acoustic pressure inside cavities can be decomposed into a series using mode shapes as base functions. Second, problems related to the acoustic intensity inside cavities require an accurate prediction of the velocity of the particles, which is directly related to the sound pressure distribution [11]. Third, accurate information on the mode shape gives rise to many direct applications. For instance, Succi [9] noticed that the position of a minimum resonant pressure in an automobile cabin can be changed, so as to improve the driver's and the passengers' comfort. All these applications are based on an accurate prediction of the modal sound distribution.

The objective of the present paper are twofold: 1) to provide a further assessment of the approach by having a closer look at the modal pressure distribution inside cavities and developing criteria for a better use of the method; and 2) to propose alternatives to improve the original approach.

In different studies, J. Pan [12–14] pointed out that using a rigid-wall mode expansion for the sound field does not always describe correctly the particle velocity or pressure gradient where absorptive or flexible part of the cavity boundary is assumed. It is known that in using such approach, although the pressure distribution in the interior domain can be accurately predicted, inaccurate results can be obtained for modeling impedance on the vibrating boundary, as determined by Gibbs' phenomenon in the Fourier series. Jayachandran et al. studied these inaccuracies and proposed a particular solution approach, which allows one to retain the advantages of the modal solution technique without compromising its accuracy [15].

In solving a one dimensional sound field problem bounded by a soft acoustic impedance using Lagrangian function, Pan [16] introduced the concept of extended mode shape function to tackle the same problem. This problem is likely to occur when the integro-modal approach is applied, because of the assumed flexible surface connecting two adjacent sub-cavities. To handle it, an improved integro-modal approach similar to the concept proposed by Pan [16] is developed. The sound pressure is still expanded over rigid-wall modes, but the selected base functions must allow a non-zero velocity over the connecting membranes. For this purpose, a slight overlap is permitted among the regular bounding cavities. It can be shown that this technique can greatly improve the accuracy of the prediction for the modal pressure and velocity distribution.

In the first step, the original integro-modal theory is briefly summarized with a special focus on how to select the base functions. The difference between the present formulation and the previous one is specified as the concept of overlapped bounding cavities is introduced in the general equations. A standard eigenvalue problem is then established. Numerical results are then presented and discussed, which show reasonably good results with the original approach, yet further improvement is obtained thanks to the modified integro-modal method.

2. Theoretical developpement

2.1. Basis for the integro-modal approach

An irregular shaped cavity, with acoustically rigid walls, is treated as a sum of connected sub-cavities, regular or not, separated by an elastic membrane as shown in Fig. 1. As most investigations did in the past, we assume that the cavity has no damping and absorption inside. Morse and Feshbach [17] stated that in each sub-volume V, the interior pressure Ψ satisfies the Green integral equation with associated boundary conditions on the enclosing surface S.

$$\Psi(r) = \int_S \left(G(r, r_0) \frac{\partial \Psi(r_0)}{\partial n} - \Psi(r_0) \frac{\partial G(r, r_0)}{\partial n} \right) \mathrm{d}S \tag{1}$$

r and r_0 are the observation and source points in the cavity respectively. The boundary conditions over the flexible membrane is determined by continuity of the normal air particle velocity and the structural velocity on the separating surface, noted S_F. Hence

$$\frac{\partial \Psi}{\partial n} = -\rho_f \dot{w} \quad \text{on} \quad S_F \tag{2}$$

where n is the normal to the surface of the boundary (positive outwards) and w is the flexural displacement of the separating membrane. ρ_f is the air density within the cavity. The flexible portion of S refers only to the separating membrane between two
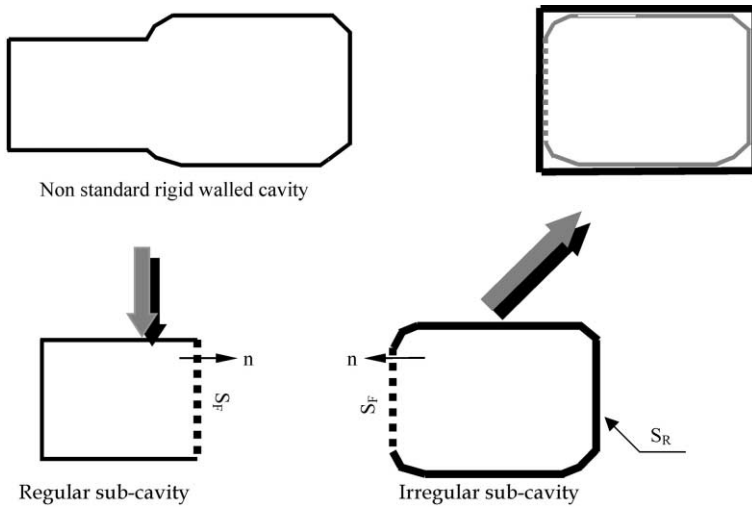
Fig. 1. Discretization of a non-standard acoustical cavity using integro-modal approach.

adjacent sub-cavities. Anywhere else on the remaining surface, noted S_R, the pressure gradient is zero.

Each sub-volume is treated separately. To construct the Green function G and the solution, the initial sub-volume V is enclosed in a larger bounding volume V_b (Fig. 1), of standard geometry and with rigid walls S_b. The modal characteristics (Φ_n ω_n) of V_b are obtained analytically, then used as base functions to express Ψ and G in an orthogonal expansion, as in Ref. [17]:

$$G(r, r_0) = \sum_n \frac{c^2 \Phi_n(r)\Phi_n(r_0)}{(\omega_n^2 - \omega^2) V_b \Lambda_n} \tag{3}$$

$$\Psi(r, t) = \rho_f c_f^2 \sum_n \frac{a_n(t)}{\Lambda_n} \Phi_n(r) \tag{4}$$

Where c is the speed of sound in air; Λ_n is the generalised mass of the n th normal mode of V_b. a_n are unknown coefficients and

$$\delta_{n,n'} \Lambda_n^2 = \int_{V_b} \Phi_n(r)\Phi_{n'}(r)\mathrm{d}V$$

More will be discussed later on the selection of the bounding cavity. Similarly, the flexural displacement of the membrane w can be expanded in terms of base function φ_m defined over the region S_F:

$$w = \sum_m q_m(t)\varphi_m \tag{5}$$

where m is the structural modal indices; $q_m(t)$ are the structural modal coordinates.
Eq. (1) is an integral equation for general time dependence. Assume

$$a_n(t) = a_n e^{i\omega t} \tag{6}$$

Knowing the orthogonal properties of the base functions, and the boundary conditions, then using the modal expansions in Eqs. (3)–(5), the integral equation Eq. (1) becomes:

$$\left(\omega_n^2 - \omega^2\right)a_n + \frac{c^2}{V_1}\sum_{n'}\frac{a_{n'}}{\Lambda_{n'}}T_{n',n} = \omega^2\frac{S_f}{V_b}\sum_m q_m L_{nm} \tag{7}$$

$$T_{n',n} = \int_S \Phi_{n'}\frac{\partial \Phi_n}{\partial n}\,\mathrm{d}s \quad L_{nm} = \frac{1}{S_F}\int_{S_F}\Phi_n\left(r_o^S\right)\varphi_m\left(r_o^S\right)\mathrm{d}S \tag{8}$$

where $T_{n',n}$ is the spatial coupling between the nth and the n'th acoustic modes of the bounding cavity and L_{nm} the modal spatial coupling coefficient between the mth base function of the membrane and the nth acoustic mode.

Furthermore, by assuming a mass-less and stiffness-free membrane, it was demonstrated in Ref. [6] that the equation describing the flexural motion of the separating membrane is reduced to the following:

$$\int_{S_F}\Psi^+\varphi_m\mathrm{d}s - \int_{S_F}\Psi^-\varphi_m\mathrm{d}s = 0 \tag{9}$$

where Ψ^+ and et Ψ^- are the sound pressure at each side of the membrane. It can be noticed that the above expression represents a global continuity of the pressure due to the integrals involved and therefore indicates a pure opening between two adjacent sub-cavities.

The key relations for solving the internal acoustic distribution in the cavity are Eqs. (7) and (9). These coupled acoustic-structural equations form an eigenvalue system, ω^2 being the unknown eigenvalue. For each eigenvalue, there is a corresponding eigenvector given by the coefficients a_n and q_m. All series expansions used in the calculations of G, Ψ and w have to be truncated, in order to implement a numerical procedure.

2.2. Selecting the base functions

2.2.1. The original approach and its limitations

As stated above, the rigid-wall modes of a standard shaped cavity V_b are used as base functions to describe the cavity sound field in normal mode expansion. In a two-dimensional case, the bounding cavity may be rectangular, circular, or of any other shape as far its modal characteristics are known. In practical application, to ensure good accuracy, the selected bounding cavity must fit, as much as possible, the

geometrical shape of its corresponding enclosed sub-cavity V. For an automobile cabin, rectangular boxes seem to be a good option [9], but for an aircraft, circular geometry would be more appropriate [10].

In a standard geometry, V and V_b coincide, as well as their respective boundary surfaces S and S_b. S_b having acoustic rigid walls, the normal derivative of Φ_n along S (S_b) is zero. Using Φ_n as the cavity normal modes and base functions for the series expansion of $\Psi(r,t)$ and $G(r_0,r)$, it is found that $\partial \Psi/\partial n = 0$ and $G/n = 0$ along the entire surface S. Consequently $T_{n,n'} = 0$, which simplifies Eq. (7). However, most studied cavities can't be conceptually dismantled into regular sub-cavities only. Irregular ones must be dealt as well. Selecting the convenient bounding cavity thus becomes an important part of the method. It was suggested earlier that the shape of the bounding cavity, should fit, as much as possible, the corresponding enclosed sub-cavity. Considering this, for a given subdivision, it seemed suitable so far (see irregular sub-cavity in Fig. 1), that the derived opening surface (S_f) should be a member of S_b, the bounding sub-cavity's boundary,

i.e. $S_f \subset S_b$

Again, using the normal modes expansion of the acoustic pressure based upon the eigenmodes (Φ_n) of V_b, the following results can be established:

$$\left(\frac{\partial \Phi_n}{\partial n}\right)_{S_b} = 0 \ \Rightarrow \ \left(\frac{\partial \Phi_n}{\partial n}\right)_{S_f} = 0 \ \Rightarrow \ \left(\frac{\partial \Psi}{\partial n}\right)_{S_f} = 0$$

Yet the boundary condition of the particle velocity $\partial \Psi/\partial n$ has been defined as non-zero by Eq. (2) which was derived from structural considerations. Relying on the observation made in Ref. [6], it is expected that the speed of convergence of the expansion (of pressure and pressure gradient) to the exact value may be affected in the vicinity of the assumed flexible membranes. As a result, the prediction accuracy in the whole multi-connected cavity could also be compromised. The effect of this inevitable handicap will be further discussed along with the numerical results.

2.2.2. The "overlapped cavities" option

To handle the expected zero-gradient obstacle, one should select base functions that satisfy the inhomogeneous boundary condition on the membrane surfaces S_F. In contrast to the previous approach, the bounding cavity is lengthened so that its boundary does not cover the membrane surfaces S_F, but permits a certain degree of overlapping. α is defined as the ratio of the additional length to the original length (related to the original approach) of the bounding cavity in the direction normal to the separating membrane surfaces (Fig. 2). Whereas adjacent bounding cavities were previously stuck together along their connecting surfaces, a slight overlap is allowed among them in the new approach, for which reason α is called the overlapping ratio. In each sub-cavity, the base functions are now related to the extended bounding cavity and are expressed in terms of the selected coordinates system and α. The term $\partial G/\partial n$ must be retained in the whole sub-cavity boundary. Taking $\alpha = 0$ leads us back
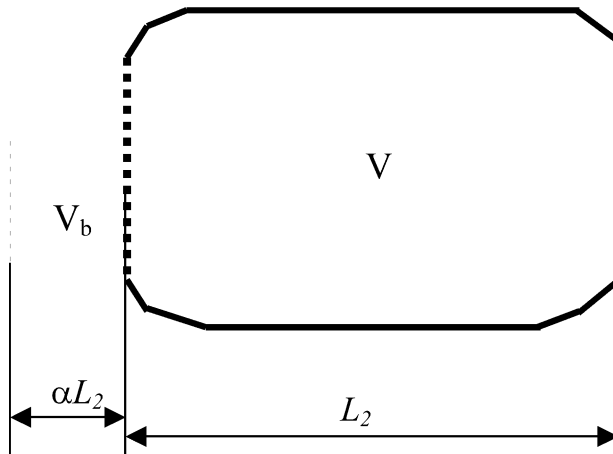
Fig. 2. Selection of extended bounding cavity for the 'overlapped cavities' approach.

to the classical approach. The integrals in Eq. (8) can be calculated numerically or analytically, depending on the complexity of the sub-enclosure shape.

2.2.3. Relation between the original and the modified integro-modal approach

For illustration purpose, rectangular bounding cavities will be used hereafter. To stress the relation between the original integro-modal approach and the one using overlapped cavities, the integrals are computed for a rectangular box with sides of length L_x and L_y in x and y directions respectively.

Let us use two adjacent bounding cavities of dimensions $L_y \times (1+\alpha)L_1$ and $L_y \times (1+\alpha)L_2$ [$\alpha = 0$ represents the real rectangular cavity of dimension $L_y \times (L_1 + L_2)$]. In Cartesian coordinates, the connecting membrane is defined by equation $x = L_1$. The first sub-cavity of volume V_{01} will have the following modes and properties:

$$\Phi_n(x, y) = \cos\left(\frac{n_x \pi x}{(1+\alpha)L_1}\right) \times \cos\left(\frac{n_y \pi y}{L_y}\right) \tag{10}$$

$$\frac{\partial \Phi_n}{\partial n}\Big|_{S_F} = -\frac{\partial \Phi_n}{\partial x}\Big|_{x=L_1} = \frac{n_x \pi}{(1+\alpha)L_1} \times \sin\left(\frac{n_x \pi}{1+\alpha}\right)\cos\left(\frac{n_y \pi y}{L_y}\right) \tag{11}$$

S_{01} and S_{b1} coincide everywhere apart from the connecting panel S_F. Hence $\Phi_n(x, y)$ can now satisfy the Neuman homogeneous boundary condition on the rigid part of S_{01} and the inhomogeneous condition on S_F. The coupling between then nth mode and the n' th mode in Eq. (8) can be calculated:

$$T_{n,n'} = \int_{So_1} \Phi_{n'} \frac{\partial \Phi_n}{\partial n} ds = \int_{S_F} \Phi_{n'} \frac{\partial \Phi_n}{\partial n} ds = \frac{n_x \pi}{(1+\alpha)L_1} \times \sin\left(\frac{n_x \pi}{1+\alpha}\right)$$
$$\times \int_0^{L_y} \cos\left(\frac{n'_y \pi y}{L_y}\right)\cos\left(\frac{n_y \pi y}{L_y}\right)dy \tag{12a}$$

$$T_{n',n} = \frac{n_x \pi L_y}{(1+\alpha)L_1} \times \sin\left(\frac{n_x \pi}{1+\alpha}\right) \times \left(\frac{1}{2} + \frac{1}{2}\delta_{0,n_y}\right)\delta_{n'_y,n_y} \tag{12b}$$

If $\alpha = 0$, $T_{n,n'} = 0$, thus, the addition of α has the effect of coupling the acoustic modes of the bounding cavities in their respective enclosed sub-cavities.

The flexural displacement of the flexible membrane can be represented by any set of orthogonal functions providing they are complete in the region of the membrane surface. In Ref. [6], following base functions been used:

$$\varphi_m(y) = \sin\left(\frac{m\pi y}{L_y}\right) \tag{13}$$

Hence

$$L_{nm} = \cos\left(\frac{n_x \pi}{1+\alpha}\right) \times \int_0^{L_y} \cos\left(\frac{n_y \pi y}{L_y}\right)\sin\left(\frac{m\pi y}{L_y}\right)dy \tag{14a}$$

$$L_{nm} = -\cos\left(\frac{n_x \pi}{1+\alpha}\right) \times \frac{m\left((-1)^{n_y+m}-1\right)}{\pi\left(n_y^2 - m^2\right)}L_y \tag{14b}$$

if $n \neq m$; $L_{nm} = 0$ if $n_y = m$ or $n_y = 0$

As the base function form an infinite set, the systems of linear equations are of infinite order. A truncation to a finite order is thus required to obtain a numerical solution. Such an approximation has been widely justified in different studies [9,18] whenever normal mode expansions were concerned.

2.3. The truncated generalized system

To illustrate how the method works for a general case, a four sub-cavity system of irregular shape is treated. Eq. (7) is applied in each sub-system k ($k = 1, 2, 3, 4$) and Eq. (9) for the $k-1$ separating membranes between adjacent sub-volumes. The procedure yields a system of linear equations that describes the coupling between Ψ and W vectors. Ψ and W are the acoustic and structural modal amplitudes, respectively, of the multi-connected model. Subscript k or $k-1$ will stand for the membrane indices and superscripts for the cavity.

$$A^k\{\Psi^k\} - \omega^2\big(I^k\{\Psi^k\} + Q_k^k\{W_k\}\big) = 0 \qquad k = 1 \tag{15a}$$

$$A^k\{\Psi^k\} - \omega^2\big(I^k\{\Psi^k\} + Q_k^k\{W_k\} - Q_{k-1}^k\{W_{k-1}\}\big) = 0 \qquad k = 2,\, N_{\text{cav}} \text{ or } = 3 \tag{15b}$$

$$A^k\{\Psi^k\} - \omega^2\big(I^k\{\Psi^k\} + Q_{k-1}^k\{W_{k-1}\}\big) = 0 \qquad k = N_{\text{cav}} = 4 \tag{15c}$$

where

$$[A^k]_{ij} = \big(\omega_i^k\big)^2 \delta_{ij} + \frac{c^2}{V_b^k \Lambda_j^k} T_{j,i}^k \quad [I^k]_{ij} = \delta_{ij} \quad \Big[Q_{k_2}^{k_1}\Big]_{ij} = \frac{S_{k_2 F}}{V_b^{k_1}} L_{i_{k_1}, j_{k_2}}; \tag{15d}$$

In the above equations, $[Q]$ is the coupling matrix. With N_{cav} sub-cavities, the first equation applies to the first and the last sub-cavity having only one separating membrane, while the second equation hold for all intermediate sub-cavities delimited by two membranes at each side. Equations on the membrane vibrations yield the following matrix form:

$$H_k^k\{\Psi^k\} - H_k^{k+1}\{\Psi^{k+1}\} = 0 \qquad k = 1,\, 2, \ldots N_{\text{cav}} - 1 = 3 \tag{16a}$$

$$\Big[H_{k_2}^{k_1}\Big]_{ij} = \frac{1}{\Lambda_j^{k_1}} L_{i_{k_1}, j_{k_2}} \tag{16b}$$

where H include terms related to the inter-modal coupling between each set of adjacent sub-cavities.

The use of bisection method gave undesirable poles, which are not the eigenvalues of the system. To avoid this problem, the system will be treated as a whole hereafter. Upon assembling the entire system, a standard eigenvalue problem is obtained as follows:

$$\big(K + \omega^2 M\big)\{F\} = 0$$
$$\{F\} = \big\{\Psi^1,\ W_1,\ \Psi^2,\ W_2, \ldots, \Psi^{N_{\text{cav}}-1},\ W_{N_{\text{cav}}-1},\ \Psi^{N_{\text{cav}}}\big\}^T \tag{17}$$

$$K = \begin{pmatrix} A^1 & 0 & 0 & 0 & 0 & 0 & 0 \\ H_1^1 & 0 & H_1^2 & 0 & 0 & 0 & 0 \\ 0 & 0 & A^2 & 0 & 0 & 0 & 0 \\ 0 & 0 & H_2^2 & 0 & H_2^3 & 0 & 0 \\ 0 & 0 & 0 & 0 & A^3 & 0 & 0 \\ 0 & 0 & 0 & 0 & H_3^3 & 0 & H_3^4 \\ 0 & 0 & 0 & 0 & 0 & 0 & A^4 \end{pmatrix} \quad M = \begin{pmatrix} I^1 & Q_1^1 & 0 & 0 & 0 & 0 & 0 \\ 0 & 0 & 0 & 0 & 0 & 0 & 0 \\ 0 & Q_1^2 & I^2 & Q_2^2 & 0 & 0 & 0 \\ 0 & 0 & 0 & 0 & 0 & 0 & 0 \\ 0 & 0 & 0 & Q_2^3 & I^3 & Q_3^3 & 0 \\ 0 & 0 & 0 & 0 & 0 & 0 & 0 \\ 0 & 0 & 0 & 0 & 0 & Q_3^4 & I^4 \end{pmatrix}$$

where M is the inertia matrix, K is the stiffness matrix and F is the eigenvector of the system with all the unknown coefficients and its components. For each eigenvalue, an eigenvector can be obtained. The components of this eigenvector are used to describe the distribution of the corresponding acoustical mode.

3. Numerical results and validation

3.1. Assessment of the original integro-modal approach ($\alpha = 0$)

A simple rectangular cavity is first used to test the method. Analytical solutions available for this configuration provide a good basis for comparison purposes. Actually, the analysis for this simple model will mostly focus on the prediction of the modal pressure distribution mainly in the vicinity of connecting surfaces. The rectangular cavity used will have dimensions: $Lx \times Ly = 2.0 \times 1.1$ m; the two-sub-cavities system will first be discussed. Lx_k and Ly_k ($k = 1,2$) are the dimensions of sub-cavity number k in the directions x and y. $Lx_1 = 0.81$, $Lx_2 = 1.19$ and $Ly_1 = Ly_2 = Ly = 1.1$. The connecting zero-mass and stiffness-free membrane between the two sub-cavities will be therefore located at $x_1 = 0.81$. When $\alpha = 0$, the bounding cavity selected to construct the base functions in each sub-cavity will have the same dimensions as its corresponding enclosed sub-volume

For a two-dimensional problem, two indices corresponding to the two orthogonal directions are involved for each acoustic mode. Their respective maximum value is denoted Nx and Ny. In all calculations reported hereafter, these two indices are always set equal: $Nx = Ny = Na$. As far as the membrane is concerned, only one index is used. M_s stands for the maximum number of terms in the structural decomposition series. Two different base functions can be used for the membrane. One is the sine function as proposed in our previous work [1] ($\varphi_m(y) = \sin\left(\frac{m\pi y}{Ly}\right), m = 1, 2, 3, \ldots M_s$), while the other is a cosine function ($\varphi_m(y) = \cos\left(\frac{m\pi y}{Ly}\right), m = 0, 1, 2, 3 \ldots M_s$). Effects of using different base functions will be discussed later.

3.1.1. Normal modes (natural frequency and mode shape)

Numerical results for the rectangular box are compared with the exact solution. Although many details on the natural frequency calculation can be found in Ref. [6], this brief section gives a general idea of the accuracy of the method. The first 10 natural frequencies, listed in Table 1, are compared with the analytical solutions. Good estimation is observed even for a small numbers of terms. The error depends on the resonant mode, and the number of terms in the expansion. As expected, the results for the resonant frequencies are more accurate as the number of modes in the expansion is increased. The numbers of the base function of the membrane regulates essentially the pressure continuity between the two adjacent sub-cavities as per Eq. (9).

Table 1
Natural frequencies of a rectangular cavity calculated with integro-modal approach (five acoustic and opening modes, two sub-cavities)

	Mode order	Exact solution (Hz)	$N_a = 5$ (Hz)	$N_a = 8$ (Hz)	$N_a = 12$ (Hz)
1	(1,0)	85.7	89.4	87.9	87.5
2	(0,1)	155.9	155.9	155.9	155.91
3	(2,0)	171.5	174.0	173.0	172.5
4	(1,1)	177.9	179.7	179.0	178.6
5	(2,1)	231.8	233.7	232.9	232.5
6	(3,0)	257.25	261.8	259.9	259.0
7	(3,1)	300.8	304.7	303.1	302.3
8	(0,2)	311.8	311.8	311.8	311.8
9	(1,2)	323.4	324.4	324.0	323.8
10	(4,0)	343.0	357.1	351.5	348.4

Fig. 3 depicts a typical contour plot of the pressure field distribution, computed with 25 terms (i.e. $N_a = 5$) in the expansion. The lines of equal sound pressure are calculated for the mode (1,2), the 10th mode at 324.4 Hz (exact value is 323.4 Hz). The sound pressure amplitude was normalized to its maximum value in the cavity. The contour plot shows good agreement with exact distribution in major part of the cavity. However, errors between exact and numerical solutions depend on the position where the amplitude is evaluated. Maximum error is observed in the vicinity of the connecting surface between the two sub-cavities. In fact, although the membrane ensures continuity of the pressures at both sides, the equal pressure lines are visibly different from the exact solutions. This phenomenon can be better seen in Fig. 4, in which the sound field distribution in the direction normal to the membrane surface at $y = 0.49$ is investigated when different number of the decomposition terms are used in sub-cavities. The discontinuous slope at the separation area was expected
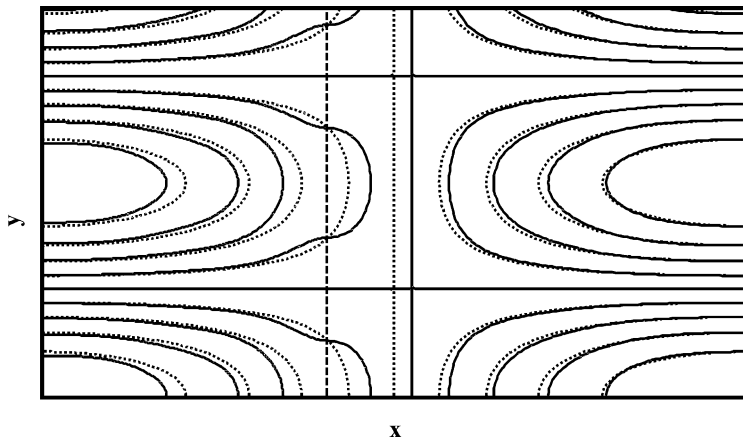
Fig. 3. The calculated lines of equal sound pressure for a rectangular cavity with $N_a = M_s = 5$. - - - - - Exact results (324 Hz), ——— Integro-modal analysis (323.4 Hz).

from the analysis made in 2.2.1. In fact, the Green's function for each sub-volume satisfies the second-order homogeneous condition on the aperture surface; thus leads automatically to a zero pressure gradient along the area of interest. It can been seen from Fig. 4 that the speed of convergence of the expansion (of the slope of the function) to the exact value will depend on the number of terms in the expansion and the position chosen for the evaluation. Near the connecting boundary, more terms may be needed to achieve the convergence. But only a few terms can give a good estimation away from such flexural panel. This observation suggests the use of a large number of decomposition terms, increasing such significantly the size of the matrices to be treated.
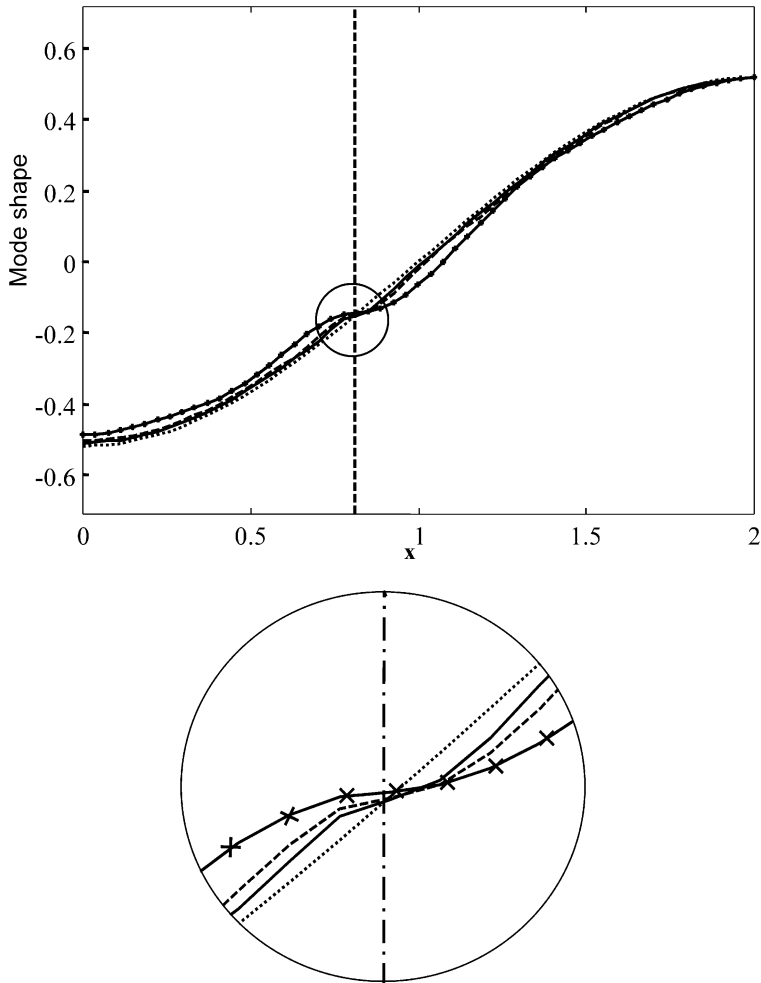
Fig. 4. Longitudinal sound field distribution (normalised by maximum value in the cavity) of the 10th acoustic modes (1,2) of a rectangular cavity ; $N_a = M_s = 5$. - - - - Analytical solution, $\times-\times N_a = M_s = 4$, $--$ $N_a = M_s = 8$. ——$N_a = M_s = 12$.

3.1.2. Particle velocity

Moreover, the non-uniform convergence of the pressure gradient doesn't allow us to estimate the values of the particle velocity by normal derivation of the pressure expansion, but using the structural solution for the particle velocity in the flexible panel according to Eq. (2). The velocity distribution along the flexible surface has been plotted in Fig. 5 for two different configurations. One option is to use the sine base functions; the other choice is to use cosine functions, in order to agree with the mathematical expression of the sound pressure expansion as was stated above. Obviously the second option agrees much more with the analytical solution and seems to be a good alternative at least as far as a rectangular bounding cavity is concerned. Hence the pressure gradient estimation on the membrane surface agrees with the exact value when its relation to the particle velocity is considered.

Increasing the number of terms improves the convergence of the velocity expansion in the inter-cavity connection, and of the sound pressure anywhere in the cavity. Hence, Ψ and $\partial\Psi/\partial n$ can be determined anywhere in the cavity. It was pointed [8] that expression [Eq. (4)] is still suitable for calculating the pressure itself throughout the cavity and everywhere on the wall surface, including the flexible portion (referring here to the connecting aperture); and this despite the non-uniform convergence of the normal derivative of the pressure expansion. Altogether the previous assessment suggests that the original integro-modal approach can achieve good convergence both for the natural frequencies and the natural mode shapes. Yet, it is clear that the discontinuity of $\partial\Psi/\partial n$ affects the convergence not only near the opening surface, but also in the whole cavity.
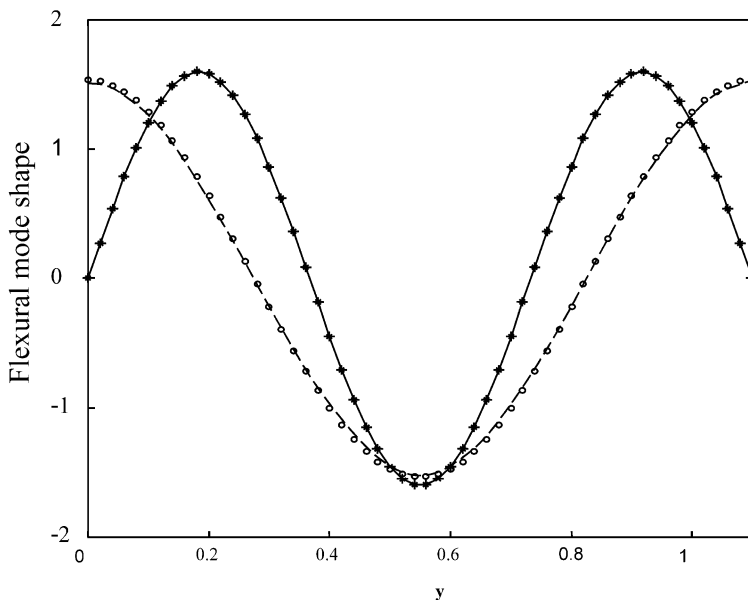
Fig. 5. Structural velocity distribution for the connecting membrane surface. - - - - Analytical result, ×−× present approach with sine base functions, ○−○−○ Present approach with cosine base functions.
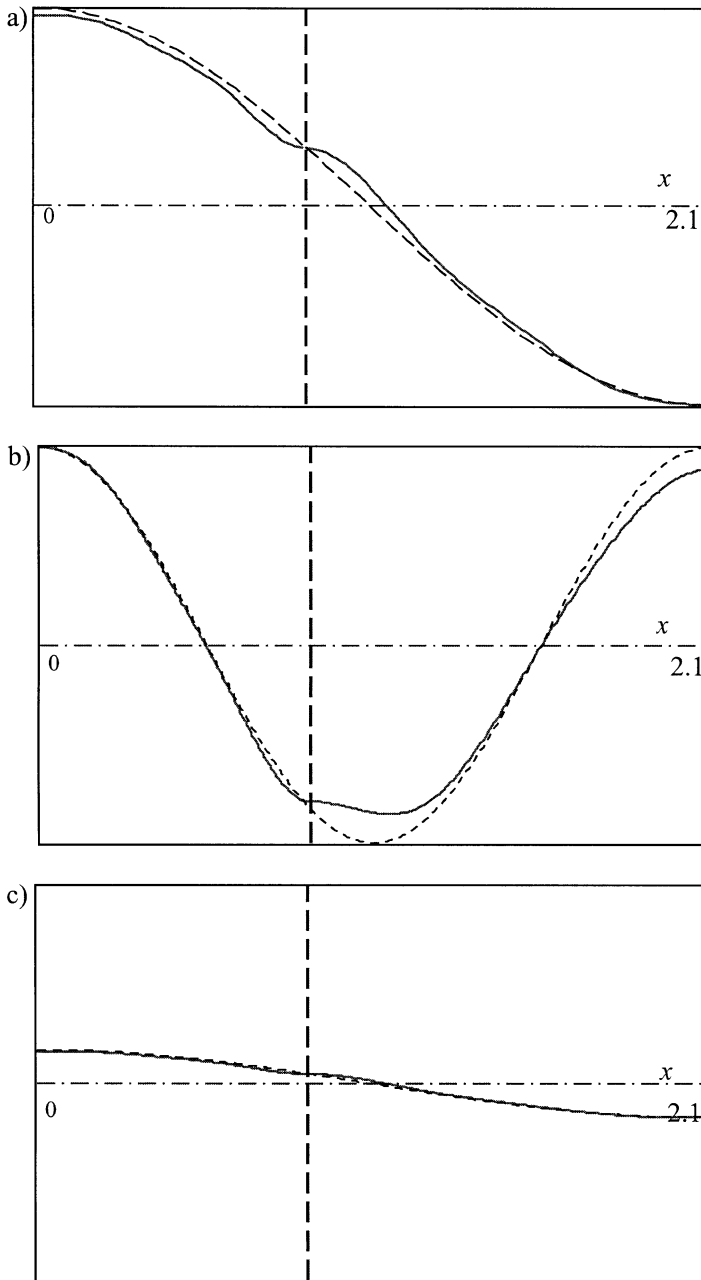
Fig. 6. Longitudinal modal sound field distribution (normalised by maximum value in the cavity) and for the first acoustic modes of a rectangular cavity, $N_a = M_s = 5$. – – Analytical results, —— integro-modal distribution. (a) $F_{exact} = 85.7$ Hz, $F_{IMM} = 89.4$ Hz; (b) $F_{exact} = 171.5$ Hz $F_{IMM} = 174$ Hz; (c) $F_{exact} = 178$ Hz $F_{IMM} = 180$ Hz.
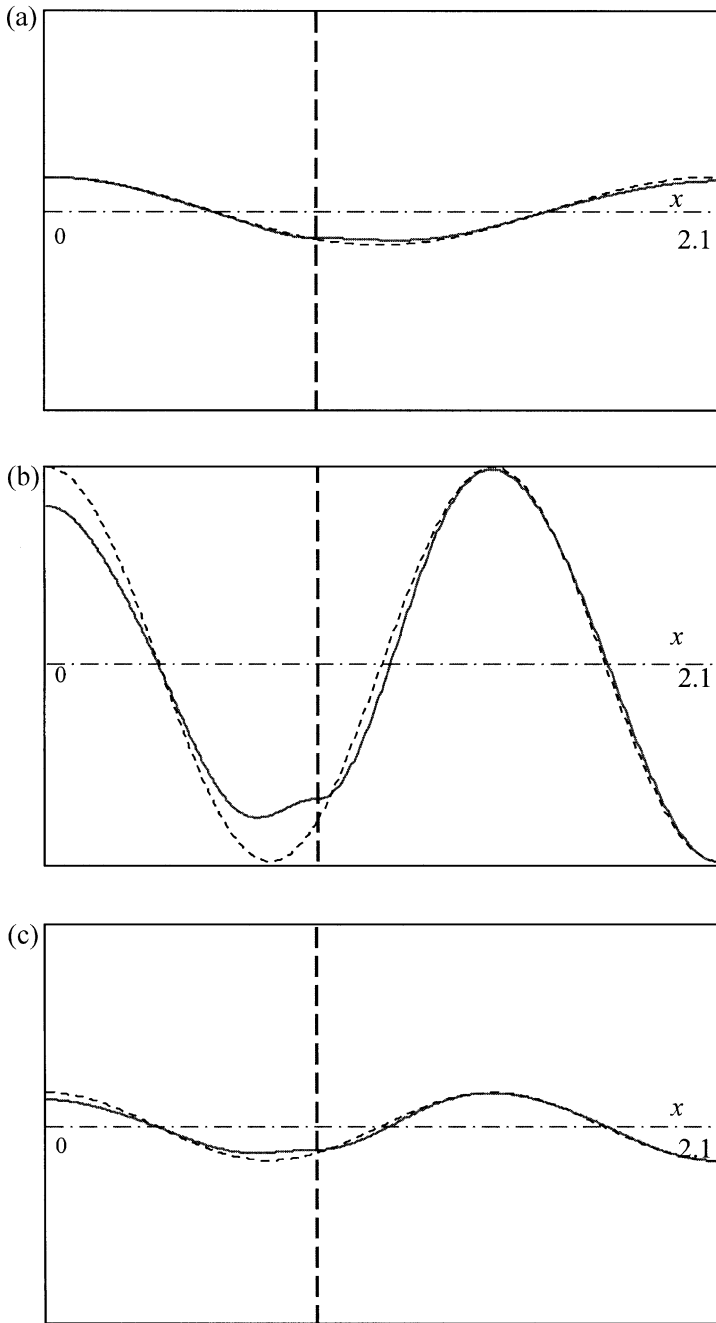
Fig. 7. Longitudinal modal sound field distribution (normalised by maximum value in the cavity) for a rectangular cavity, $N_a = M_s = 5$. – – Analytical results, —— integro-modal distribution. (a) $F_{exact} = 232$ Hz, $F_{IMM} = 234$ Hz; (b) $F_{exact} = 257$ Hz, $F_{IMM} = 262$ Hz; (c) $F_{exact} = 301$ Hz, $F_{IMM} = 305$ Hz.

More results are given in Figs. 6 and 7, in which a number of selected modes are investigated. It can be noticed that when $\partial\Psi/\partial n$ is near zero throughout the opening wall [see modes (1,1) and (2,1)], best resolution is achieved for the sound pressure distribution and natural frequencies prediction. In the meanwhile, lower convergence in the cavity occurs for the mode (3,0) when discontinuity of pressure gradient is steeper. These observations suggest a way of improving the prediction in certain cases: when dividing the acoustic enclosure, one should for any specific natural mode, if convenient, locate the opening walls where minimum gradient is expected.

Increasing the number of sub-cavities also affect the accuracy of the prediction. In Fig. 8 the sound field distribution of the rectangular cavity is investigated for a two and a four subdivisions model using the same number of terms. The latter generates much better results in the whole cavity than the two sub-cavities case.

3.2. The modified integro-modal approach using overlapped cavities

The modified approach is tested using the same configuration with a two-connected sub-cavities system. Eq. (17) was solved for different overlapping rates, with only few acoustic modes and membrane terms ($N_a = M_s = 5$). The resulting estimation of mode (1,2) frequency was plotted in Fig. 9, using a value of $\alpha = 8\%$. A comparison with Fig. 3 reveals the improvement brought by the use of overlapped cavities. In fact, the calculated distribution of sound pressure agrees well with the exact distribution in the whole cavity. Comparing with Fig. 3, there is no more irregularity near the connecting aperture. By allowing the inhomogeneous condition
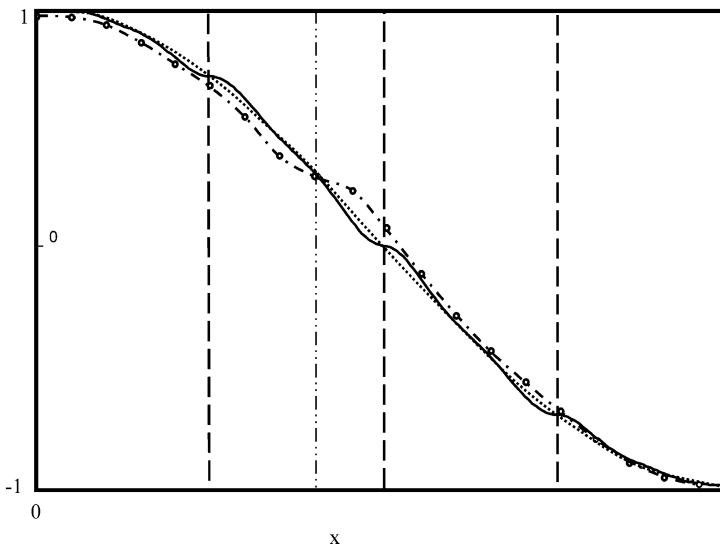
Fig. 8. Sound field distribution of the first acoustic mode of a rectangular cavity divided in two or four subcavities. Exact and approximated results with $N_a = M_s = 5$ flexural modes. - - - Analytical result, —○— present approach (two sub-cavities), –present approach (four sub-cavities), ··········-boundary line (two sub-cavities), ————boundary lines (four-sub-cavities).
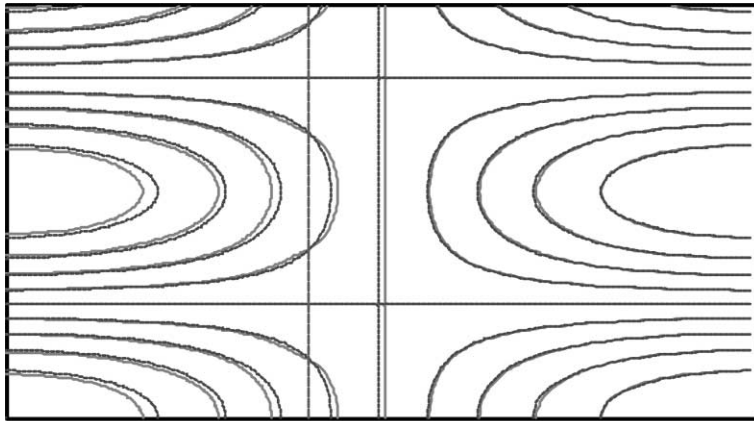
Fig. 9. Calculated lines of equal sound pressure amplitude for a rectangular cavity with $N_a = M_s = 5$, $\alpha = 8\%$; mode (1,2). - - - Exact results, ————IMM analysis.

in the separating opening, the numerical sound pressure can adjust itself to satisfy the boundary condition of the pressure gradient or velocity continuity. Consequently, the discontinuity of slope has dropped considerably.

The influence of α is significant particularly near the opening boundary. In fact, for each configuration, it exists an optimal value of α to ensure a good accuracy in terms of natural frequencies. In the present case, Fig. 10 shows the sensitivity of the natural frequency on the α value, with the optimal value being $\alpha = 8\%$. The contour
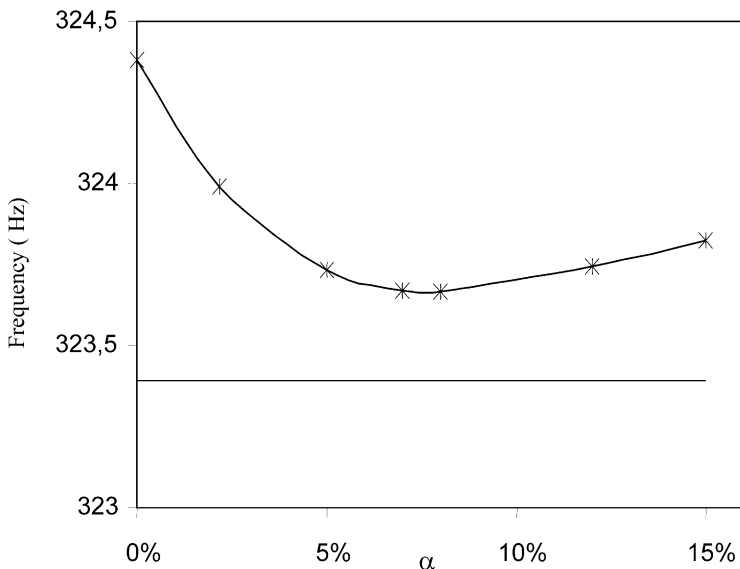
Fig. 10. Evaluated resonnant frequencies of a rectangular cavity, mode (1,2) versus overlapping ratio and $N_a = M_s = 5$. - * - * - Integro-modal approach, Exact solution.

plot of the sound field in Fig. 11 confirms the relevance of the selected rate for good convergence where maximum error for the sound field is observed when $\alpha = 0$. This error is significantly reduced with $\alpha = 8\%$. Beyond 8% the bounding cavities are too distorted from the real sub-cavities to give a reasonable approximation.

The square of the amplitude error between the approximated sound field distribution and exact solution in the cavity (Fig. 12), reveals that the technique of overlapped cavities also helps to improve the convergence of the standard integro-modal solution, without increasing the number of base functions in the expansions. This can be very convenient when dealing with systems of more complex shapes.
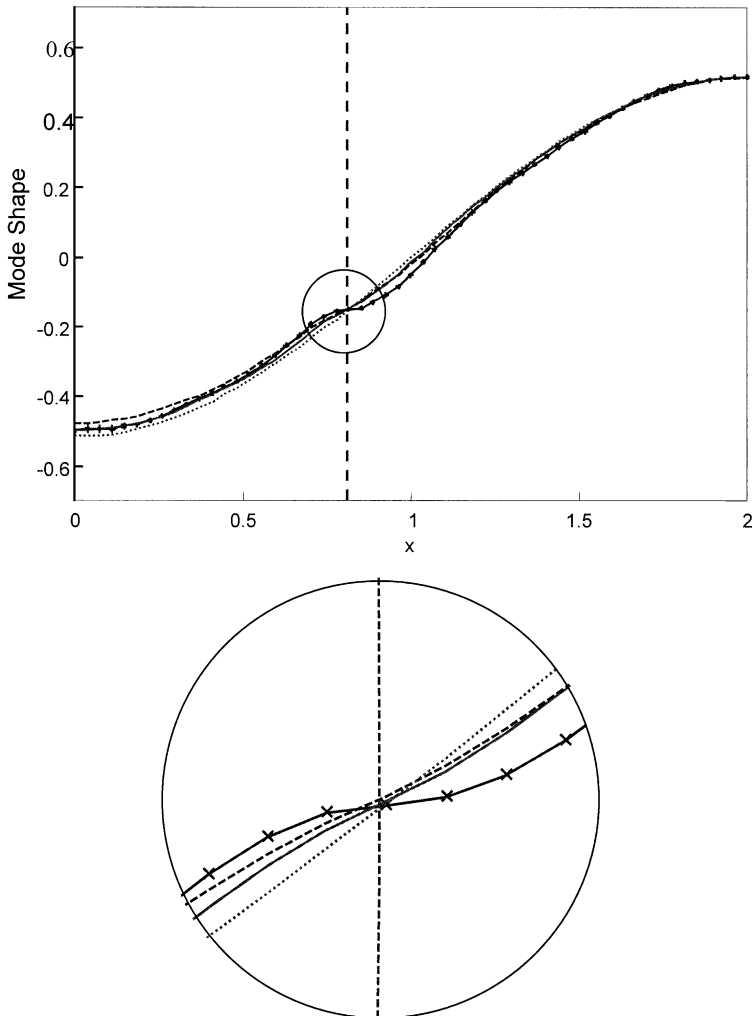
Fig. 11. Longitudinal sound field distribution (normalised by maximum value) of a rectangular cavity; modes (1,2); $N_a = M_s = 5$ and $\alpha = 8\%$. Analytical solution, $-\times-\times-$, $\alpha = 0\%$ —, $\alpha = 8\%$, $--\alpha = 15\%$.
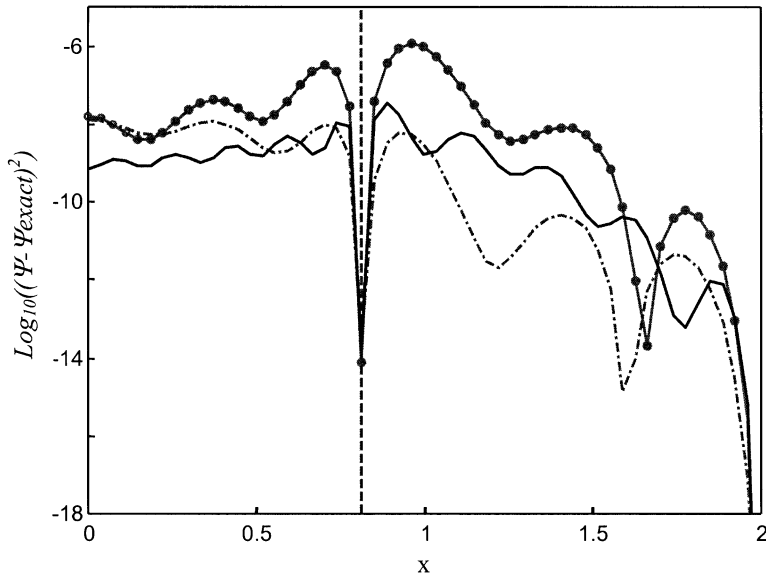
Fig. 12. Square of the amplitude error between the approximated sound field distribution and exact solution of the first modal pressure. $-\bigcirc-$ $N_a = M_s = 5$, $\alpha = 0\%$, ——$N_a = M_s = 10$, $\alpha = 0\%$ — — $N_a = M_s = 5$, $\alpha = 8\%$.

Tests with irregular acoustic enclosures will be necessary to complete the assessment of the reliability of the integro-modal approach.

3.3. Validation with a trapezoidal cavity

In order to understand how the method works for an irregular cavity, a trapezoidal cavity is considered. Hamery and Dupire [19] stressed the need for investigating acoustic fields in trapezoidal cavities with very strong shape perturbation. They worked on devices involving trapezoidal shaped cavities having an angle between adjacent walls close to 55°. In Ref. [20], experimental and finite element methods were used to calculate the first three acoustic modes of a trapezoidal cavity with a deviation of 54°. The estimation is based on the finite element method using triangular elements. The same trapezoidal cavity is considered in the present paper as an example for calculating the normal acoustic modes, using the modified integro-modal approach. The cavity can be separated in two regions. One is rectangular and the other is triangular. Acoustic properties of the former region are determined, using the normal modes of the rectangular cavity (extended if $\alpha > 0$). As there is no analytical solution for the triangular enclosure, it is conceptually dismantled in four sub-cavities. Again rectangular bounding cavities are chosen to describe the modal properties in each sub-cavity. In short, the whole cavity is divided in five rectangular sub-volumes. Five acoustic and membrane terms in each sub-cavity were proved to give a reasonable estimation of the first frequencies. For higher frequencies, more acoustic modes and membrane terms should be used.

In Fig. 13 the lines of constant pressure are drawn, corresponding to the first three modes of the trapezoidal cavity. The pressure amplitude is normalized by its maximum value. 0.2 units of pressure amplitude differentiate two successive lines. The nodal lines are clearly indicated. The lines outside the cavity have no physical significance, but they illustrate how the method works, i.e. approximates the acoustic pressure using rigid-wall modes of rectangular sub-cavities. On the left-hand side a zero-overlapping ratio was considered, then a non-zero ratio on the right. As expected, numerical solutions with zero-overlapping show discontinuous slopes of the acoustic pressure lines across the connecting panels. The generated error due to the slope discontinuity is increased in the nearby of such areas and propagates eventually in the entire cavity. With the use of over-lapping cavities (5%), the curving of the pressure amplitude lines is apparently smoother compared to the $\alpha = 0$ case. Numerical tests for the three modes of interest revealed that, using a ratio beyond 5% does not give any noticeable change in the pressure amplitude approximation. In Table 2, results in terms of natural frequencies are tabulated. Comparisons with finite element and experimental method are also provided. The agreement is excellent whether α is 0 or 6%. In Fig. 14, simulation results with and without overlapping are compared to both FE results and experimental results. Again, no overlapping was used for the left-hand side figures and then a 5% overlapping ratio for the right-hand side ones. Improvement brought by the use of a 5% overlapping
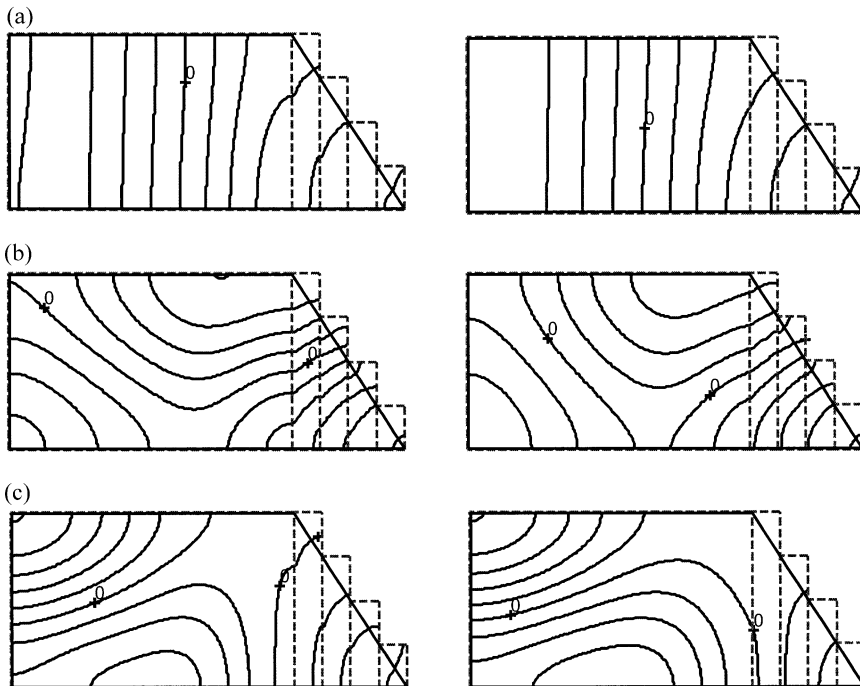
Fig. 13. Lines of constant acoustic pressure amplitude (normalised to maximum value) in a trapezoidal cicular cavity; (a) first mode; (b) second mode; (c) third mode: left: $\alpha = 0\%$; right: $\alpha = 5\%$.

Table 2
Natural frequency for a trapezoidal cavity (five acoustic and opening modes, five sub-cavities)

	Present analysis		Experimental results	Finite element method
	$\alpha = 0\%$	$\alpha = 6\%$		
First mode (Hz)	93.4	91.0	93.0	92.5
Second mode (Hz)	165.1	162.4	164.0	162.5
Third mode (Hz)	182.2	180.0	182.0	179.1
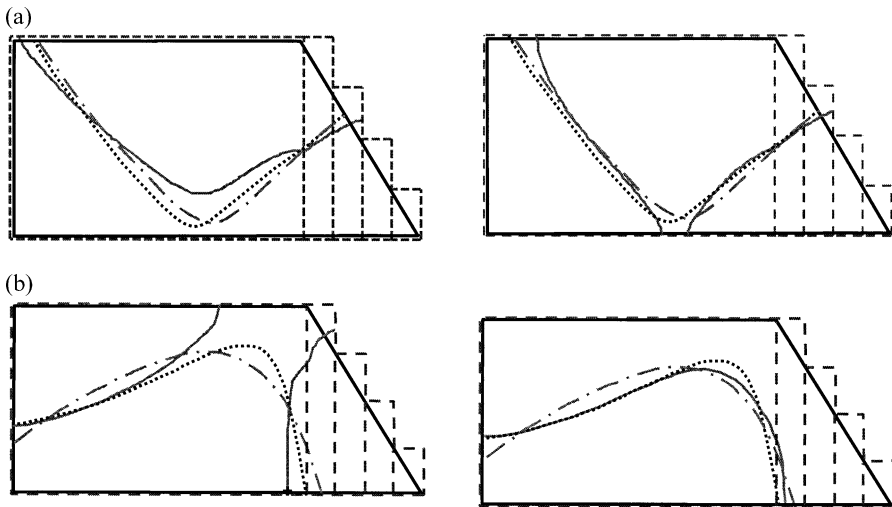
Fig. 14. nodal lines of trapezoidal cavity; (a) second mode; (b) third mode: left: $\alpha = 0\%$; right $\alpha = 5\%$. - - - Finite elements results, ————Integro-modal results,———Experimental results, – – – -Sub-cavity boundary line.

is obvious especially for the third mode (Fig. 13b). In fact, original IMM ($\alpha = 0\%$) fails to give an acceptable prediction of the sound pressure with two segments of lines split out, whilst the improved method gives very nice agreement with the two reference cases.

4. Conclusions

The original Integro-Modal Method was assessed through investigation of mode shapes. It was established that the selected base functions reveal the limitations of such an approach. A zero pressure gradient was imposed on the surface separating two adjacent sub-cavities, whereas its true value was proportional to the non-zero particle velocity. Because of such discontinuity, the convergence of the pressure was affected in the vicinity of opening apertures and eventually in the whole cavity. In

order to handle the obstacle, an improved technique, based on the use of extended bounding cavities, was proposed. The new base functions related to the extended sub-cavities permitted a non-zero gradient between adjacent sub-cavities. Numerical tests were performed either with the zero-ratio or the non-zero-ratio model. It was observed that:

- The original approach allowed a good prediction of the natural frequency of cavities. In terms of the sound pressure prediction, however, the accuracy of the original approach is questionable in the vicinity of the junctions between sub-cavities. The use of a non-zero-overlapping ratio helped to solve or at least attenuate the problem of gradient discontinuity between adjacent sub-cavities without altering the good accuracy in the frequency estimation.
- By minimizing the discontinuity of slope, the improved method also helped to improve the convergence of sound pressure in the whole cavity.
- Satisfactory results could be achieved with very limited number of acoustic modes in the series expansion, when one introduces a non-zero ratio.

Actually, the above results illustrated how the extended approach can help deal with the problem of discontinuous gradient and achieve better convergence, providing a proper selection of the different parameters, namely the number of sub-cavities, the number of acoustic and structural modes per each sub-cavity, and the overlapping ratio. From the presented examples, it is clear that there is no general or analytical role, including all engineering designs, to calculate the optimal choice of the parameters of convergence. Each mode has to be handled individually. Whilst Ref. [6] established a standard procedure to determine the optimal number of sub-cavities and acoustic and structural base functions, the choice of α involves however successive numerical tests. Some useful information can be obtained in the work of Pan [21], which shows that the optimal range of α is related to the orthogonal properties of the base function. Whether this statement is applicable to the present situation requires further investigations.

As a final remark, some problems which go beyond the assumptions of the present paper are briefly mentioned. The extension of the present approach to 3D problems involving vibrating boundary should be possible, although complications due to the possible strong irregularities in all three dimensions are foreseeable. As mentioned before, modeling of the vibrating boundary should be coupled to the acoustic modeling of the cavity. Since acoustic treatment based on the modal solution leads to inaccurate estimation of the velocity, usual practice is to use the vibration equation for this purpose [8]. The original IMA has already been applied to the case of a simplified 3D aircraft fuselage involving vibrating structures and an irregular-shaped cabin [10,22]. Modifications proposed in the present paper should not affect the applicability of the method in this regard. Moreover, possible present of absorption material on the wall can be simulated using the local reacting impedance model as outlined in Ref. [23]. Further investigations on other cases involving sharp geometrical discontinuities are still needed to have a more overall assessment of the method.

Acknowledgements

References

[1] Brebbia AA, Telles JCF, Wrobel LC. Boundary element techniques. New York: Springer; 1984.
[2] Easwaran V, Craggs A. An application of acoustic finite element models to finding the reverberation times of irregular rooms. Acustica 1996;82:54–64.
[3] Missaoui J, Cheng L. A combined integro-modal approach for predicting acoustic properties of irregular-shaped cavities. J Acoust Soc Am 1997;101:3313–21.
[4] Levine H. Acoustical cavity excitation. J Acoust Soc Am 2001;109:2555–65.
[5] Kang SW, Lee JM. Eigenmode analysis of arbitrarily shaped two-dimensional cavities by the method of point-matching. J Acoust Soc Am 2000;107:1153–60.
[6] Kim YY, Kim DK. Applications of waveguide-type base functions for the eigenproblems of two-dimensional cavities. J Acoust Soc Am 1999;106:1704–11.
[7] Amir N, Starobinski R. Finding the eigenmodes of two dimensional cavities with two axes of symmetry. Acustica 1996;82:811–23.
[8] Dowell EH, Gorman III GF, Smith DA. Acousto-elasticity: general theory, acoustic natural modes and forced response to a sinusoidal excitation including comparison with experiment. J Sound and Vib 1977;52:519–41.
[9] Succi GP. The interior acoustic field of an automobile cabin. J Acoust Soc Am 1987;81:1688–94.
[10] Missaoui J, Cheng L. Vibroacoustic analysis of a finite cylindrical shell with a floor partition. J Sound Vib 1999;226(1):101–23.
[11] Cheng L, Nicolas J. Radiation of sound into a circular cylindrical enclosure from point-driven plates with general boundary conditions. J Acoust Soc Am 1992;91(3):1504–13.
[12] Pan J, Bies DA. The effect of fluid-structural coupling on sound waves in an enclosure—theoretical part. J Acoust Soc Am 1990;87(2):691–707.
[13] Pan J. A note on the prediction of sound intensity. J Acoust Soc Am 1993;93:1641–4.
[14] Pan J. A second note on the prediction of sound intensity. J Acoust Soc Am 1995;97:691–4.
[15] Jayachandran V, Hirsch SM, Sun JQ. On the numerical modelling of interior sound field by the modal function expansion approach. J Sound Vib 1998;210:243–54.
[16] Pan J. A third note on the prediction of sound intensity. J Acoust Soc Am 1999;105:560–2.
[17] Morse PM, Feshbach H. Methods of theoretical physics, vol. II. New York: McGraw-Hill; 1953.
[18] Ouellet D, Guyader J-L, Nicolas J. Sound field in a rectangular cavity in the presence of a thin, flexible obstacle by the integral equation method. J Acoust Soc Am 1991;89(5):2131–9.
[19] Hamery P, Dupire P, Bruneau M. Acoustic fields in trapezoidal cavities. Acta Acustica 1997;83:13–18.
[20] Shuku T, Ishihara K. The analysis of the acoustic field in irregular shaped rooms by the finite element method. J Sound Vib 1973;29:67–73.
[21] Pan J. Approximating eigensolutions of distributed structures using the adjustable quasi comparison functions. In: Proceedings of the 5th International Congress on Sound and Vibration, Adelaide, December 1997. pp. 2411–8.
[22] Li DS, Cheng L, Gosselin CM. Analysis of structural acoustic coupling of a cylindrical shell with an internal floor partition. J Sound Vib 2002;250(5):903–21.
[23] Cheng L, Lesueur C. Preliminary study on vibroacoustic model scaling of a structure coupled to an acoustic cavity. J Acoustique 1990;3:349–59.